Photonuclear Disintegration at High Energies (<350 MeV)*

T. A. GABRIEL† AND R. G. ALSMILLER, JR.

Oak Ridge National Laboratory, Oak Ridge, Tennessee 37831

(Received 17 February 1969)

Calculations of high-energy $(40 \lesssim E_\gamma \lesssim 350$ MeV) photon-nucleus $(A \gtrsim 12)$ collisions have been carried out. The results of the initial interaction of the photon with the nucleus are obtained either from Levinger's quasideuteron model or, when energetically possible, from one of the four-pion–nucleon states formed in photon-nucleon interactions. The effect of nucleon- (pion-) nucleus interactions that follow the initial photon interaction is taken into account by using an intranuclear-cascade model. The results of the calculations are compared with a variety of experimental data, and good agreement is obtained.

INTRODUCTION

EARLY theoretical calculations of high-energy ($\gtrsim 50$ MeV) photonuclear interactions failed to predict a sufficient intensity in the high-energy end of the nucleon-emission spectra. This failure led Levinger[1] to introduce the quasideuteron model. He assumed that an incident photon is absorbed in the nucleus by a neutron-proton pair in a state of high relative momentum. He showed that there exists an approximate relationship between the cross section for the absorption of a photon by this neutron-proton pair, a quasideuteron, and the cross section for the photodisintegration of a true deuteron. Since its introduction, a variety of calculations[1-7] have been done using this model. In all of these calculations, however, the interaction of the neutron-proton pair after absorption with the rest of the nucleus has either been neglected or drastically approximated. In this paper, photonucleon-production spectra are calculated using the quasideuteron model and taking into account in a systematic manner all secondary interactions. The calculations are carried out by utilizing Monte Carlo methods.

Except for the use of a more detailed nuclear model, the quasideuteron model is used in the present calculations in essentially the same form as in the calculations mentioned above. The constant that appears in the relation between the cross section for the absorption of a photon by a quasideuteron and the cross section for the absorption of a photon by a deuteron is assumed to be a universal constant, that is, independent of both photon energy and atomic mass. In all of the calculations which are compared with experimental data, the value

of 10.3 given by Garvey et al.[8] for this constant has been used, because this value was found to give the best agreement with experimental data.

The secondary interactions between the nucleons and the remaining nucleus after the photon absorption process were included by means of the intranuclear-cascade model proposed by Serber[9] and utilized by several authors, Metropolis et al.[10] and Bertini.[11] The Bertini results were explicitly used in the present calculations.

For photon energies above the pion threshold, pion production competes with photon absorption by a quasideuteron as a possible initial interaction. Therefore, single-pion production was introduced into the present calculations through photon-nucleon interactions which led to a pion-nucleon state. All secondary interactions of this pion and nucleon with the remaining nucleus were also included using the intranuclear-cascade model.

In the intranuclear-cascade model as employed here, an excited compound nucleus remained after the cascade calculation was completed. The contribution to the particle-emission spectra due to the deexcitation of this excited compound nucleus was taken into account by using an evaporation model.[12-14] The use of this model also makes it possible to calculate the cross sections for the production of the various residual nuclei.

It will be shown by comparing with a wide variety of experimental data that the calculational model employed here is capable of yielding reliable results over a large range of atomic mass numbers ($\gtrsim 12$) and over a wide range of photon energies $(40 \lesssim E_\gamma \lesssim 350$ MeV). It is also known that the contribution of the secondary nucleon-nucleus and pion-nucleus interactions is large, so that calculations in which these interactions are neglected have very limited validity.

[1] J. S. Levinger, Phys. Rev. **84**, 43 (1951).
[2] K. G. Dedrick, Phys. Rev. **100**, 58 (1955).
[3] Kurt Gottfried, Nucl. Phys. **5**, 557 (1958).
[4] S. Fujii, Nuovo Cimento **25**, 995 (1962).
[5] Robert J. Cence and Burton J. Moyer, Phys. Rev. **122**, 1634 (1961).
[6] T. I. Kopaleishvili and R. I. Jibuti, Nucl. Phys. **44**, 34 (1963).
[7] J. L. Matthews, dissertation, Massachusetts Institute of Technology, 1967 (unpublished).

[8] J. Garvey et al., Nucl. Phys. **70**, 241 (1965).
[9] R. Serber, Phys. Rev. **72**, 1114 (1947).
[10] N. Metropolis et al., Phys. Rev. **110**, 185 (1958).
[11] H. W. Bertini, Phys. Rev. **131**, 1801 (1963).
[12] V. F. Weisskopf, Phys. Rev. **52**, 295 (1937).
[13] I. Dostrovsky et al., Phys. Rev. **116**, 683 (1959).
[14] L. Dresner, Oak Ridge National Laboratory Report No. ORNL-CF-61-12-30, 1961 (unpublished).

DESCRIPTION OF CALCULATIONS

Nuclear Model

The nuclear model used in the photonuclear calculations is exactly the same as the one used in the Bertini calculations[11] and will be described only briefly here.

The nucleon density distribution inside the nucleus was determined from the experimental work of Hofstadter.[15] He was successful in fitting electron scattering data using a nuclear-charge density distribution of the type

$$\rho(r) = \frac{\rho_1}{\exp[(r-c)/z_1]+1}, \tag{1}$$

where the parameters c and z_1, used in the calculations, have the values $1.07\times10^{-13}A^{1/3}$ cm and 0.545×10^{-13} cm, respectively. To approximate this continuous charge distribution, the nucleus was divided into three concentric spheres. The density in each sphere was uniform, and it was set equal to the average value of the Hofstadter charge density distribution in the corresponding region of the nucleus. The outer radius of each region was given by solving the equation

$$\rho(r) = \alpha_i\rho(0), \qquad i=1, 2, 3 \tag{2}$$

where $\alpha_1=0.9$, $\alpha_2=0.2$, and $\alpha_3=0.01$, that is, by solving for the radii at which the density is 90, 20, and 1% of its value at the center.

The above charge density distribution was assumed to apply equally well for the proton and neutron density distribution, but the neutron-to-proton density ratio for any given region is equal to the ratio of neutrons to protons for the entire nucleus. The normalization constant ρ_1 was calculated to make the total number of protons in the three regions equal to the atomic number of the nucleus.

A form of the Fermi distribution was used for the momentum distribution of the nucleons inside the nucleus. The protons (neutrons) in each region were assumed to have a zero-temperature Fermi distribution of the type

$$f_i(p) = (8\pi w_i/h^3\rho_i)p^2, \tag{3}$$

where w_i is the number of protons (neutrons) in the ith region and ρ_i is the proton (neutron) density in the ith region. The normalization on $f_i(p)$ requires that

$$\int_0^{p_{f_i}} f_i(p)\,dp= \text{total number of protons (neutrons)} \tag{4}$$

in the ith region,

where p_{f_i} is the Fermi momentum for protons (neutrons) in the ith region.

When handled in this way, the entire momentum distribution of the nucleus no longer represents a true zero-temperature Fermi distribution but can be roughly approximated by a Maxwell-Boltzmann distribution with a kT value of 15 MeV.[16-18]

The binding energy of the most loosely bound nucleon within the nucleus was taken to be 7 MeV. Therefore, the depth of the potential for protons (neutrons) was given by the appropriate Fermi energy plus 7 MeV for each of the three regions. The pion potential was arbitrarily assumed to be equal to the potential of the nucleon with which the pion was interacting. The photons were assumed to be unaffected by the nucleon potential. As particles crossed potential boundaries, kinetic energy was added or subtracted depending upon the relative depth of the two potential regions. All things considered, however, the total energy of the system remained constant.

Photon-Quasideuteron Interaction

Using the method of Heidmann[19] for treating the neutron-proton pair within the nucleus and assuming that prior to the absorption of the photon the pair enters a state roughly corresponding to the $^3S_1$ ground state of the deuteron, Levinger[1] showed that the cross section for the absorption of a photon by a quasideuteron moving within a nucleus is given approximately by

$$\sigma_{\text{QD}}= (L/A)\sigma_D, \tag{5}$$

where σ_D is the cross section for the photodisintegration of the deuteron, A is the atomic mass number, and L is the quasideuteron constant which is independent of A number and photon energy. The convention adopted by Levinger[1] for the evaluation of the photodeuteron cross section was continued here, that is, σ_D is evaluated in the rest frame of the quasideuteron system. Levinger obtained the value of 6.8 for L, but in most of the calculations presented here, the experimental value of 10.3 obtained by Garvey et al.[8] was used since this was found to give the best agreement with the experimental results. An average of the experimental values was used for the photodeuteron disintegration cross sections.[7,20-22]

To determine the position in the nucleus where the photon is absorbed, it is necessary to know the quasideuteron density as well as the total cross section. The determination of this density is not straightforward, because it is not clear how protons and neutrons in different regions of the three-region nucleus should be paired to form a quasideuteron. If pairs with members in different regions are included, the determination of the proper volume element for calculating the quasideuteron density is problematic. This difficulty in mind, it was decided that each of the three nuclear regions would be treated independently; that is, the quasi-

[15] R. Hofstadter, Rev. Mod. Phys. **28**, 214 (1956).

[16] L. S. Azhgirey et al., Nucl. Phys. **13**, 258 (1959).
[17] J. D. Dowell et al., Proc. Phys. Soc. (London) **75**, 24 (1960).
[18] J. M. Wilcox and B. J. Moyer, Phys. Rev. **99**, 875 (1955).
[19] J. Heidmann, Phys. Rev. **80**, 171 (1950).
[20] F. Partovi, Ann. Phys. (N.Y.) **27**, 79 (1964).
[21] A. V. Tollestrup and J. C. Keck, Phys. Rev. **101**, 360 (1956).
[22] R. Ching and C. Schaerf, Phys. Rev. **141**, 1320 (1966).

deuteron density in each region would be determined by pairing all neutrons and protons in a given region. However, when this is done, the total number of neutron-proton pairs in the nucleus is not equal to NZ, where N is the number of neutrons and Z is the number of protons in the nucleus. This causes no conceptual difficulty, but it means that the constant L in Eq. (5) has a different definition than it has had in previous quasideuteron calculations. To avoid this, the quasideuteron density in the ith region was calculated as

$$\frac{(Nf_iV_i)(Z\rho_iV_i)}{V_i} \Bigg/ \sum_{j=1}^{3} \rho_j^2V_j^2 = NZ(\rho_i^2V_i/\sum_{j=1}^{3}\rho_j^2V_j^2),$$

(6)

$$\sum_{i=1}^{3} \rho_iV_i = 1,$$

(7)

where ρ_i is the nucleon density and V_i is the volume, of the ith region; that is, the quasideuteron density was renormalized so that the total number of neutron-proton pairs considered in the entire nucleus becomes NZ. The renormalization factor

$$\sum_{i=1}^{3} \rho_i^2V_i^2$$

is slightly A-dependent, varying from 0.6 at $A=10$ to 0.4 at $A=200$, so the L as used here still has a slightly different definition than that used in previous quasideuteron calculations.

From the cross section for a photon-quasideuteron interaction and the number density of the quasideuteron, a point within the nucleus where the interaction takes place may be obtained by standard sampling procedures.[23] The point selected is dependent on the momenta of the neutron $(\mathbf{p}_{ni})$ and proton $(\mathbf{p}_{pi})$ which make up the quasideuteron since the cross section is evaluated in the rest system of the quasideuteron, that is, in the system in which $\mathbf{p}_{ni}'+\mathbf{p}_{pi}'=0$. The determination of the energy and momenta of the neutron and proton following the photon absorption poses a slight problem because the processes of photon absorption by a deuteron and photon absorption by a quasideuteron are not on the same energy shell; that is, for a given incident photon energy, the total energy associated with each process is not necessarily the same. This difference in total energy is due to the positive relative energy of the neutron-proton pair in the neutron-proton rest frame and the negative binding energy of the deuteron.

To bring a closer resemblance between the two processes at this point in the calculations, a "pseudophoton energy" was obtained by requiring the same total energy in the center of mass associated with each process. This pseudophoton energy was used only to obtain a more "realistic" polar center-of-mass emergent angle for the proton and was not used directly in the

kinematics for obtaining the final energies and momenta of the proton and neutron after the absorption of the photon. In this way, the two processes were brought into a closer correspondence but yet conservation of energy and momentum was maintained in the quasideuteron calculations.

If the deuteron is initially at rest and $\omega,\boldsymbol{\omega}$ is the incident photon energy, momentum; m_p is the rest mass of the proton; m_n is the rest mass of the neutron; m_d is the rest mass of the deuteron; $\mathbf{p}_{ni}$ is the initial momentum of the neutron; $\mathbf{p}_{pi}$ is the initial momentum of the proton; $E_{ni}=(p_{ni}^2+m_n^2)^{1/2}$ is the total initial energy of the neutron; $E_{pi}=(p_{pi}^2+m_p^2)^{1/2}$ is the total initial energy of the proton, then the total energy in the center-of-mass system[24] of the photon-deuteron system is (in terms of $\omega=\omega_{\text{pseudo}}$)

$$[2(\omega_{\text{pseudo}})(m_d)+m_d^2]^{1/2},$$

(8)

and the total energy in the center-of-mass system[24] of the photon-neutron-proton system is

$$\{m_n^2+m_p^2+2[\omega(E_{ni}+E_{pi})$$
$$+E_{ni}E_{pi}-\omega(\mathbf{p}_{ni}+\mathbf{p}_{pi})-\mathbf{p}_{ni}\cdot\mathbf{p}_{pi}]\}^{1/2}.$$

(9)

Therefore, by equating Eqs. (8) and (9),

$$\omega_{\text{pseudo}} = \frac{m_p^2+m_n^2-m_d^2}{2m_d} + \frac{\omega}{m_d}[E_{pi}+E_{ni}]$$
$$+ \frac{E_{pi}E_{ni}-\omega\cdot(\mathbf{p}_{ni}+\mathbf{p}_{pi})-\mathbf{p}_{ni}\cdot\mathbf{p}_{pi}}{m_d}.$$

(10)

The initial momentum of the nucleons was obtained by sampling from the appropriate Fermi distribution, and the direction of the momentum was assumed to be isotropic. Unless otherwise noted, all quantities are measured with respect to the bottom of the nuclear well. The photon-deuteron differential cross section at this "pseudophoton energy" was then used, in conjunction with standard statistical sampling techniques, to obtain the polar center-of-mass emergent angle for the proton. For "pseudophoton energies" below 140 MeV, the theoretical differential cross section given by Partovi[20] was used, while for energies greater than 140 MeV, the experimental values of Tollestrup and Keck[21] and Matthews[7] were employed. The center-of-mass azimuthal angle ϕ was assumed to be uniformly distributed between 0° and 360°.

Using the center-of-mass emergent angles of the proton (θ, ϕ), and relativistic kinematics[24] in the center-of-mass system–defined by the photon, neutron, and proton–the final energies of the neutron and proton were determined. The Pauli exclusion principle was taken into account at this point by requiring that the kinetic energy of both the proton and neutron be above the appropriate Fermi energy. If the condition was not fulfilled, the reaction was rejected and another collision

[23] T. A. Gabriel and R. G. Alsmiller, Jr., Oak Ridge National Laboratory Report No. ORNL-TM-2481, 1969 (unpublished).

[24] K. G. Dedrick, Rev. Mod. Phys. **34**, 429 (1962).

site and type of interaction were selected as if the first selected interaction had never occurred. For the range of photon energies ($\sim$40–$\sim$350 MeV) considered in these calculations, the exclusion principle has a substantial effect. Without its inclusion, many of the calculated results presented later would be changed.

Photon-Nucleon Interactions—Pion Production

For photon energies above approximately 160 MeV, pion production becomes possible and must be included along with the quasideuteron process as a possible initial interaction. Consideration was restricted to photon energies of the order of or less than 350 MeV, so only single-pion production was considered. To define this interaction, free-photon-proton cross sections were used.[25–32] A definition of the photon-neutron interactions was obtained by the assumption of charge symmetry; thus,

$$\sigma(\gamma+p\rightarrow p+\pi^0) \equiv \sigma(\gamma+n\rightarrow n+\pi^0)$$
$$\sigma(\gamma+p\rightarrow n+\pi^+) \equiv \sigma(\gamma+n\rightarrow p+\pi^-). \quad (11)$$

For the photon-nucleon interaction the initial nucleon momentum is obtained, as before, by sampling from the appropriate Fermi distribution. Therefore, since the nucleon density and cross sections for photon-nucleon interactions are known, an acceptable intranuclear-interaction site and type of photon-nucleon interaction can be determined.[23]

For single-pion production it was assumed that the pion is emitted isotropically in the center-of-mass system defined by the photon and nucleon. This assumption was experimentally verified for photon energies up to approximately 260 MeV at which the pion differential angular distribution starts to assume a backward asymmetry.[29]

Since it was assumed that the nuclear potential acts on the pions as well as on the nucleons, arbitrary means were used so that over-all energy balance remains. The reason for this nonbalance in total energy is that free-particle kinematics do not account for the change in potential energy when the total number of particles initially affected by the field changes during interaction. A quick calculation will show that the amount of energy that cannot be accounted for in single-pion production is positive and equal to the nuclear well depth. The choice of well depth, neutron or proton, is dependent upon the type of pion-producing interaction.

To correct this anomaly so that over-all total energy is conserved in a pion-producing interaction, the final-state energies and momenta of the pion and nucleon were obtained as follows: First, preliminary energies and momenta were obtained using the center-of-mass emergent angles of the pion, (θ, ϕ), and free-particle kinematics defined in the center of mass of the photon and nucleon. Then, if V represents the appropriate well depth corresponding to the energy excess, the final-state energies of the nucleon and pion were arbitrarily increased by $V/2$.[11] The direction cosines defined by the momentum components were assumed to be unaltered.

After the final energy of the nucleon and pion was determined, the Pauli exclusion principle was taken into account by requiring that the kinetic energy of the nucleon be above the appropriate Fermi energy. If this was not the case, the calculation proceeds as if the collision did not occur.

Secondary Interactions

Once the type and site of the initial interaction have been determined and all other information needed to define the state of the reactant products has been calculated, the effect of secondary-particle–nucleus interaction was investigated. To determine this effect, the intranuclear-cascade model of Serber,[9] as developed by Bertini,[11] was used. This model assumed that the interaction between a high-energy ($\gtrsim$30 MeV) particle and a nucleus can be described on the basis of intranuclear free–particle-particle collisions. With the present photon energy range, the possible secondary interactions considered were nucleon-nucleon and pion-nucleon scattering reactions, charge-exchange reactions, and pion absorption. All necessary cross sections and a much more detailed discussion of these calculations can be found in the published works of Bertini.[11]

The type and site of secondary intranuclear particle-particle collisions were determined in the same way as was the initial interaction. Two-particle kinematics, together with experimental free-particle differential cross sections, were used in the determination of the energy and momenta of the reactants. The Pauli exclusion principle was taken into account in all secondary interactions by requiring, as before, that the kinetic energy of any nucleon involved in any reaction be above the appropriate Fermi energy.

Each of the particles resulting from any acceptable interaction was traced through the nucleus until an intranuclear collision occurred. This collision produced other particles which were traced through the nucleus. For each incident photon that has an interaction, the necessary information for a complete analysis was retained, that is, the energy of the incident photon, the type of target nucleus, the type, energy, and direction cosines of the escaping particles, etc.

When the energy of the particle following an intranuclear collision has an energy below a preset value, it was assumed that its motion could no longer be described by free-particle collisions and its energy was assumed to be shared by all the nucleons in the nucleus.

[25] D. H. White et al., Phys. Rev. 120, 614 (1960).
[26] V. L. Highland and J. W. DeWire, Phys. Rev. 137, 1293 (1963).
[27] Karl Berkelman and James A. Waggoner, Phys. Rev. 117, 1364 (1960).
[28] J. I. Vette, Phys. Rev. 111, 622 (1958).
[29] M. Beneventano et al., Nuovo Cimento 4, 333 (1956).
[30] A. V. Tollestrup et al., Phys. Rev. 99, 220 (1955).
[31] R. L. Walker et al., Phys. Rev. 99, 210 (1955).
[32] C. Freitag et al., Z. Physik 175, 1 (1963).

Thus, for each incident photon that has an interaction, there remains after the fast particles have escaped from the nucleus a residual excited nucleus. The type of residual nucleus, as well as its excitation energy, can be determined, of course, from the initial nucleus, the energy of the incident photon, and the kind and energy of the particles that escape from the nucleus.

In the calculations presented here, the deexcitation by particle emission of the compound nucleus was treated using an evaporation model. The theory of the evaporation model is originally due to Weisskopf.[12] This theory has recently been developed by Dostrovsky et al.[13] and most recently by Dresner.[14] It is Dresner's version of Weisskopf's evaporation theory that was used in the calculations.

By considering many incident photons with all possible impact parameters and analyzing statistically the information regarding the type, energy, and direction cosine of the particles that escape from the nucleus, the differential cross sections for photonucleon and photopion production may be obtained. Similarly, by analyzing the information on the residual nuclei which remain after the evaporation process is complete, the cross section for the production of a particular type of residual nucleus may be obtained.

In presenting the calculated results, the effects of secondary interactions will be shown explicitly. The nucleons and pions that make up the intranuclear cascade will be referred to as cascade nucleons and pions. The nucleons or pions involved specifically with photons will be referred to as primary cascade nucleons or pions. Once a primary cascade particle has undergone a collision, it is no longer considered to be a primary cascade particle.

RESULTS OF CALCULATIONS

Photon Spectrum and Cross-Section Normalization

Calculations have been carried out for incident monoenergetic photons and for each of the following types of incident photon spectra:

(1) The thin-target bremsstrahlung spectrum. This type of photon spectrum results when monoenergetic electrons undergo radiative scattering in a thin target ($\ll 0.1$ radiation length thick). To represent this thin-target bremsstrahlung spectrum, the theoretical expression given by Schiff[33] was used; that is,

$$\frac{d\sigma(k_{max}, k)}{dk} = \frac{2Z^2 r_0^2}{137k} \left\{ \left[1 + \left(\frac{E}{E_0}\right)^2 - \frac{2}{3}\frac{E}{E_0} \right] \right.$$

$$\times \left(\ln m(0) + 1 - \frac{2}{b}\tan^{-1}b \right) + \frac{E}{E_0}$$

$$\left. \times \left(\frac{2}{b^2}\ln(1+b^2) + \frac{4(2-b^2)}{3b^3}\tan^{-1}b - \frac{8}{3b^2} + \frac{2}{9} \right) \right\},$$

(12)

[33] L. I. Schiff, Phys. Rev. **83**, 252 (1951).

where

$$b = \frac{2E_0 E Z^{1/3}}{111k}, \qquad \frac{1}{m(0)} = \left(\frac{k}{2E_0 E}\right)^2 + \left(\frac{Z^{1/3}}{111}\right)^2,$$

E_0, E is the initial and final total energy of the electron in a collision, in $m_0 c^2$ units, k is the energy of emitted photon, k_{max} is the maximum possible energy of emitted photon, Z is the atomic number of target material, and $r_0 = e^2/m_0 c$ is the classical electron radius.

(2) The thin-target bremsstrahlung difference spectrum. If $d\sigma(k_{max}, k)/dk$ and $d\sigma(k_{max}', k)/dk$ represent two thin-target Schiff bremsstrahlung spectra with maximum photon energies of k_{max} and k_{max}', such that $k_{max} \geq k_{max}'$, and if k_{norm} represents a photon energy less than k_{max}', then the thin-target bremsstrahlung difference spectrum is defined for photon energies between k_{norm} and k_{max} by

$$\frac{d\sigma_d(k_{max}, k_{max}', k_{norm}, k)}{dk} = \frac{d\sigma(k_{max}, k)}{dk} - A\frac{d\sigma(k_{max}', k)}{dk},$$

(13)

with

$$A = \frac{d\sigma(k_{max}, k_{norm})}{dk} \bigg/ \frac{d\sigma(k_{max}', k_{norm})}{dk}, \quad k_{norm} \leq k \leq k_{max}'$$

$$= 0, \qquad\qquad\qquad k_{max}' < k \leq k_{max}.$$

The choice of k_{norm} usually depends upon the size of k_{max}' and/or on the experimental data to which the calculations will be compared. The quantity k_{norm} should be sufficiently smaller than k_{max}' so that when the difference of the two Schiff spectra is taken, photon energies below k_{norm}, which is now in the energy region where the shape of the Schiff spectrum is not very dependent on k_{max}' (or k_{max}), are substantially removed. Once this condition has been satisfied, the sensitivity of the calculations to variations in k_{norm} is small. One advantage in using the bremsstrahlung-difference techniques is that, since the low-energy photons can be removed in the energy region where the quasideuteron mechanism is not expected to apply, the calculated neutron differential energy spectrum can be extended to very low emission energies.

The following procedure was used to normalize the calculated data. For monoenergetic photons, the differential and total cross sections are normalized per incident photon. Since this analysis is statistical,

$$\frac{d^2\sigma_i(k)}{d\Omega dE} = \frac{f_i(E, \Delta E, \Omega, \Delta\Omega)}{\Delta\Omega \Delta E g},$$

(14)

where $f_i(E, \Delta E, \Omega, \Delta\Omega)$ equals the number of particles of type i emitted per second with energy in ΔE about E into the solid angle $\Delta\Omega$ ($\cong 2\pi \mid \Delta\cos\theta \mid$) about Ω by photons of energy k; g equals the incident photon flux and is obtained by dividing the geometric cross section by the number of incident photons per second. (The number of incident photons used in the calculations

depends only on the statistical accuracy needed.) For an incident bremsstrahlung difference spectrum, the calculated cross sections are also normalized per incident photon. In this case,

$$\left\langle \frac{d^2\sigma_i}{d\Omega dE} \right\rangle = \int_{k_{norm}}^{k_{max}} \frac{f_i(E, \Delta E, \Omega, \Delta\Omega)}{\Delta\Omega\Delta Eg} \frac{1}{G} \frac{d\sigma_D}{dk}$$

$$\times (k_{max}, k_{max}', k_{norm}, k) dk, \quad (15)$$

$$G = \int_{k_{norm}}^{k_{max}} \frac{d\sigma_D}{dk} (k_{max}, k_{max}', k_{norm}, k) dk. \quad (16)$$

For an incident bremsstrahlung spectrum, the differential and total cross sections are normalized per equivalent quanta; that is,

$$\left\langle \frac{d^2\sigma_i}{d\Omega dEQ} \right\rangle = \int_{0}^{k_{max}} \frac{f_i(E, \Delta E, \Omega, \Delta\Omega)}{\Delta\Omega\Delta Eg} \frac{1}{Q} \frac{d\sigma}{dk} (k_{max}, k) dk,$$

$$(17)$$

$$Q = \frac{1}{k_{max}} \int_{0}^{k_{max}} k \frac{d\sigma}{dk} (k_{max}, k) dk. \quad (18)$$

The integrals in these equations were evaluated using standard sampling techniques. The integrated cross sections are obtained by summing over the appropriate coordinates.

Even though both the calculated and experimental differential cross sections obtained using a bremsstrahlung spectrum are normalized per equivalent quanta, the comparisons of the results indicate that the normalizations are not the same. Presumably, this difference arises because the low-energy part of the Schiff spectrum, which enters into the calculations only through the normalization, is not a good representation of the low-energy photon spectrum obtained experimentally using a target of finite thickness.[34] Since the experimental photon spectrum is not known and is probably dependent on the experimental arrangement, it does not seem possible to obtain an absolute comparison between the calculations and the experimental results for the case of an incident bremsstrahlung spectrum. In all of the comparisons presented here, the calculations have been normalized to the experimental data. This was done by dividing the calculated values by

$$Q = bQ_{Schiff},$$

where

$$b = const$$

and

$$Q_{Schiff} = \text{the number of calculated equivalent}$$
$$\text{quanta using the Schiff spectra.}$$

In all cases where this renormalization has been carried out, the value of b is given. It is important to note that only one value of b is used for any particular set of experimental data.

---

[34] O. V. Bogdankevich and F. A. Nikolaev, *Methods in Bremsstrahlung Research* (Academic Press Inc., New York, 1966).

Sensitivity of Calculations to Variations of Quasideuteron Constant

Since the quasideuteron constant was the only adjustable parameter available, its effect on the calculations is of interest. There are two basic changes that might result by changing L: (1) the change in the absolute magnitude of the total and differential cross sections, and (2) the change in the relative shape of the differential cross-section spectrum.

Since the distances over which interactions are possible are so much less than the mean free path, there should exist a linear relationship between the value of the constant L and the absorption cross section. However, this will be true only in the calculations for photon energies high enough that the exclusion principle does not restrict a substantial number of interactions but low enough that pion production does not contribute.

Plotted in Fig. 1 are the energy spectra of emergent neutrons resulting from (85, 55)-MeV bremsstrahlung difference photons on ^{63}Cu for two different values of the quasideuteron constant. The two energy spectra are averaged over the angles between 62° and 72°. For this particular set of calculations $L/L' = 1.24$ ($L = 8.284$) and $[\sigma(L)_{abs}/\sigma(L')_{abs}] = 1.22$. Other calculations have been performed on different elements at different energies, but the results are similar; that is, $L/L' = [\sigma(L)_{abs}/\sigma(L')_{abs}]$. Only for an L value greater than 100 did the above relation fail substantially.
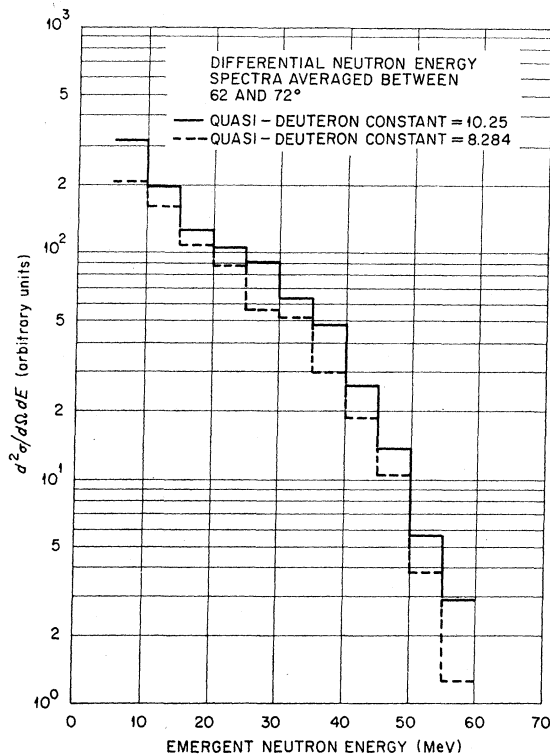
FIG. 1. Differential neutron energy spectra at 67.5° resulting from (85, 55)-MeV bremsstrahlung-difference photons on ^{63}Cu for two different values of the quasideuteron constant.

It should also be noted that the magnitude of the energy spectrum is changed and not the basic shape (when viewed on a semilogarithmic plot). This will generally be true as long as the before-mentioned conditions remain and the nuclear model is not changed.

Comparisons with Experimental Data

Comparisons between the calculations and a substantial part of the available experimental data on high-energy $(40 \lesssim E_\gamma \lesssim 350 \text{ MeV})$ photonuclear interactions are presented in the subsections to follow. The comparisons include the energy and angular distributions of emitted neutrons, protons, and charged and neutral pions; cross sections for the production of specific residual nuclei; cross sections for observing neutron and proton coincidences; π^-/π^+ ratios.

Differential Neutron Spectra from (85, 55)-MeV Bremsstrahlung-Difference Photons on Selected Elements

Recently, Kaushal et al.[35] submitted for publication neutron energy spectra at 67.5° resulting from (85, 55)-MeV bremsstrahlung-difference photons on 18 elements
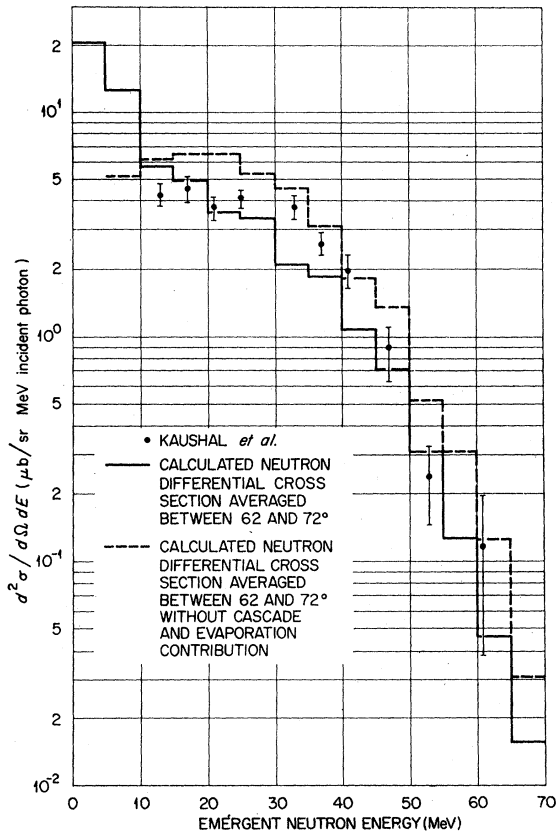
FIG. 2. Differential neutron energy spectrum at 67.5° resulting from (85, 55)-MeV bremsstrahlung-difference photons on ^{12}C.

[35] N. N. Kaushal et al., Phys. Rev. **175**, 1330 (1968).
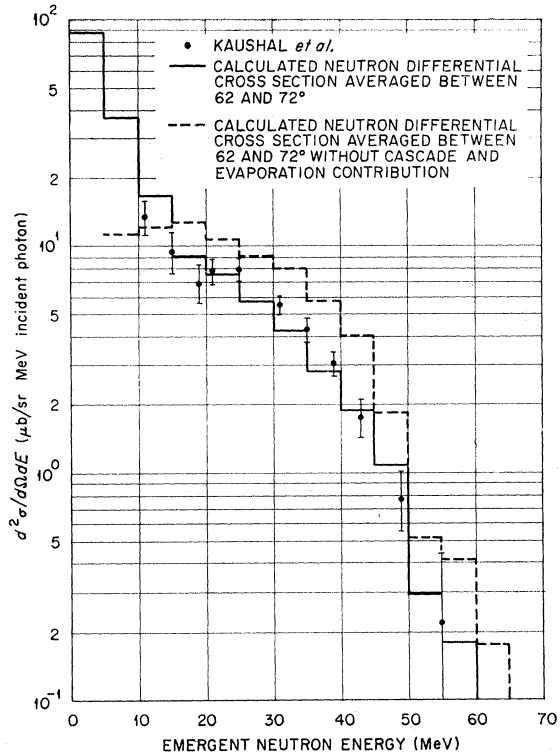
FIG. 3. Differential neutron energy spectrum at 67.5° resulting from (85, 55)-MeV bremsstrahlung-difference photons on ^{27}Al.

from Li to U. These data can give not only a good check on the combination of the quasideuteron and cascade models at the lower incident photon energies but also a good check of the combination on a substantial number of nuclei.

For comparison, the following six elements were chosen: ^{12}C, ^{27}Al, ^{63}Cu, ^{118}Sn, ^{181}Ta, and ^{207}Pb. The calculated and experimental results are shown in Figs. 2–7. The statistical errors (one standard deviation) in the calculated neutron energy spectra are approximately $\pm 12\%$. The dashed-line histogram in all the figures represents the neutron differential cross sections obtained by neglecting secondary intranuclear interactions. It should be noted that below 5 MeV (7 MeV for Pb) there is no indicated value for this primary cascade neutron differential cross section. This omission is due to the cutoff energy[11] used in the calculations. In the Bertini calculations,[11] the cutoff energy for both neutrons and protons is usually chosen to be one-half the Coulomb barrier for that nucleus. Since the evaporation calculations are not extremely sensitive to the value of the cutoff energy as long as its value is near that of the Coulomb barrier, an energy of 5 MeV (7 MeV for Pb) was chosen as an appropriate cutoff energy. The calculated neutron differential cross section with secondary interactions included is indicated in the figures by the solid-line histograms. For most cases, inclusion of the secondary nucleon-nucleus interactions through the use

FIG. 4. Differential neutron energy spectrum at 67.5° resulting from (85, 55)-MeV bremsstrahlung-difference photons on ^{63}Cu.

From the over-all agreement obtained, it appears that the lower-photon-energy data $(E_\gamma \sim 65 \text{ MeV})$ can be explained by combining the quasideuteron, cascade, and evaporation models. It should be noted again that all of these calculations were accomplished using only one value for the quasideuteron constant, $L = 10.3$, and all comparisons are on an absolute basis.

Differential Proton Energy Spectra from 110-MeV Bremsstrahlung Photons on ^{12}C

In Figs. 9–13, the calculated differential cross sections are compared with the data of Whitehead et al.[36] for emergent protons at 36.5°, 51.4°, 71.2°, 90°, and 128.6° produced by 110-MeV bremsstrahlung on ^{12}C. The calculated values have been normalized to the experimental data by dividing by 1.17 [$b = 1.17 = Q/Q_{\text{Schiff}}$

of the cascade and evaporation models brings the calculated cross sections into much better agreement with the experimental data. This, however, is not a very good check of the evaporation model, since the majority of the neutron yield above 10 MeV is due to the cascade part of the calculations.

For the ^{12}C comparisons, the calculated primary-neutron-energy spectrum has the shape closest to the experimental one. Since the cascade calculations are primarily designed for medium- and heavy-weight nuclei, any discrepancy noted here may indicate a slight failure of the calculations for very light nuclei. Over all, the agreement is best for the medium-weight nuclei, but for all nuclei the agreement is good for the lower-neutron-energy part of the spectra.

For ^{63}Cu, the contribution due to the evaporation process is shown in Fig. 8. As can be seen, this additional contribution brings the calculations into better agreement with the experimental data.

Listed in Table I are the energy-integrated neutron differential cross sections. The calculated values have been listed both with and without evaporation contribution. The agreement is quite reasonable, and, where there is an evaporation contribution, it usually improves the agreement.

FIG. 5. Differential neutron energy spectrum at 67.5° resulting from (85, 55)-MeV bremsstrahlung-difference photons on ^{118}Sn.

[36] C. Whitehead et al., Phys. Rev. **110**, 941 (1958).

(see section on photon spectrum)]. This value for b was used, since it appeared to give the best over-all agreement.

Shown with the Whitehead *et, al.*[36] data in Figs. 11 and 12 are "modified" data taken by Matthews *et al.*[37] for 100-MeV bremsstrahlung on ^{12}C. (The Matthews energy base was modified so that the results now appear to be 110-MeV bremsstrahlung data.) A substantial difference exists in the shapes of the two experimental energy spectra at the two proton emergent angles. The difference is very noticeable at the lower proton energies. The calculations, however, represent a good average of the two sets of experimental data at these two angles. Since this is one of the few experiments that has determined the energy spectrum at several angles, it should be noted that except for the 128.6° comparisons (where the error bars are large), the agreement is equally good
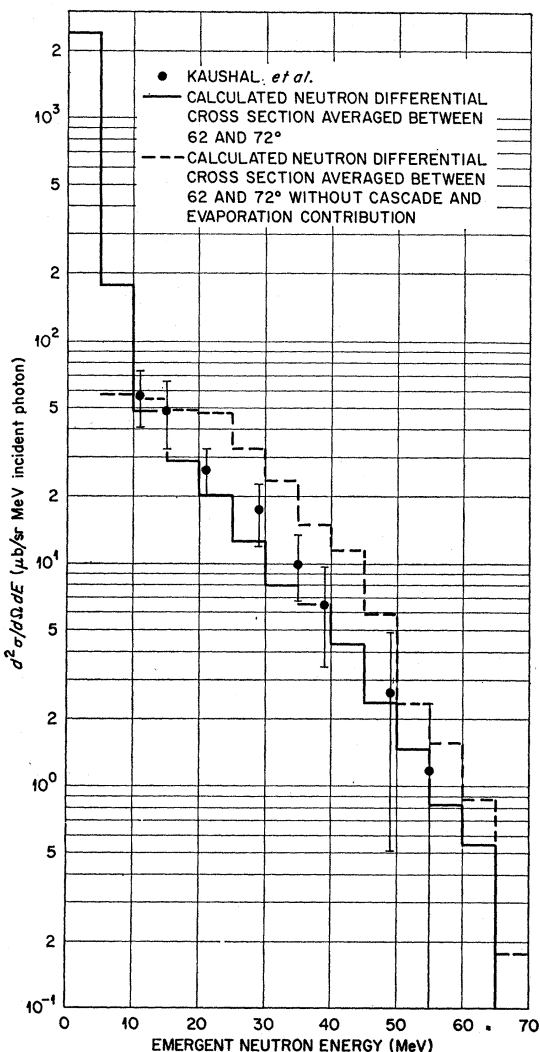
FIG. 6. Differential neutron energy spectrum at 67.5° resulting from (85, 55)-MeV bremsstrahlung-difference photons on ^{181}Ta.

[37] J. L. Matthews *et al.*, Nucl. Phys. **A112**, 654 (1968).
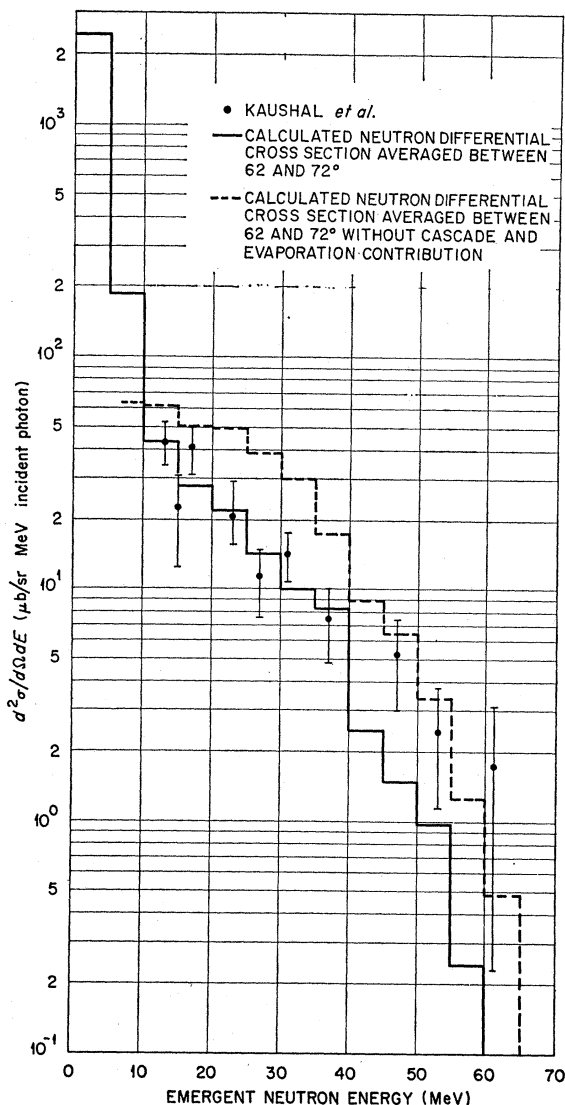
FIG. 7. Differential neutron energy spectrum at 67.5° resulting from (85, 55)-MeV bremsstrahlung-difference photons on ^{207}Pb.

at all angles. Also, in contrast to the comparisons with the Kaushal *et al.* ^{12}C data, the comparison in Figs. 9–13 do not indicate any failure of the model in light nuclei.

Differential Proton Energy and Angular Distribution Produced by 335-MeV Bremsstrahlung Photons on ^{12}C

In Figs. 14–16, the proton angular distributions resulting from 335-MeV bremsstrahlung on ^{12}C obtained by Kim *et al.*[38] for proton energies of 156, 174, and 192 MeV are compared with calculations. The calculated values have been normalized to the experimental data by dividing by 2.75 ($Q = 2.75Q_{\text{Schiff}}$). In Figs. 17 and 18, comparisons of the energy differential proton-emission cross sections are made. These figures also contain

[38] Y. S. Kim *et al.*, Phys. Rev. **129**, 1362 (1963).

TABLE I. Neutron-emission cross sections at 67.5°.[a]

Target	Lower-neutron-energy integration limit (MeV)	Integrated cross sections (mb/sr)		
		Calculated[b]		
		Without evaporation	With evaporation	Expt[c]
^{12}C	10	0.118±0.012	0.118±0.012	0.127±0.013
	20	0.066±0.010	0.066±0.010	0.087±0.013
	30	0.026±0.006	0.026±0.006	0.046±0.010
^{27}Al	10	0.211±0.021	0.246±0.025	0.224±0.023
	20	0.117±0.018	0.119±0.018	0.131±0.020
	30	0.052±0.010	0.052±0.010	0.059±0.012
^{63}Cu	10	0.334±0.037	0.374±0.037	0.345±0.035
	20	0.174±0.026	0.179±0.026	0.171±0.026
	30	0.077±0.016	0.077±0.016	0.087±0.017
^{118}Sn	10	0.454±0.045	0.485±0.049	0.559±0.060
	20	0.237±0.036	0.237±0.036	0.275±0.041
	30	0.106±0.021	0.106±0.021	0.107±0.021
^{181}Ta	10	0.648±0.065	0.669±0.067	0.851±0.085
	20	0.284±0.043	0.284±0.043	0.414±0.062
	30	0.121±0.024	0.121±0.024	0.164±0.033
^{207}Pb	10	0.632±0.063	0.650±0.065	0.658±0.066
	20	0.297±0.045	0.297±0.045	0.337±0.051
	30	0.108±0.022	0.108±0.022	0.182±0.036

[a] The photons result from the difference of two bremsstrahlung spectra with maximum energies of 55 and 85 MeV.

[b] Neutron cross sections averaged between 62° and 72°.

[c] N. N. Kaushal et al., Phys. Rev. **175**, 1330 (1968). Kaushal quotes ±15% on his over-all absolute error, so for these comparisons the experimental error is calculated as ±10% for neutron energies greater than 10 MeV, ±15% for neutron energies greater than 20 MeV, and ±20% for neutron energies greater than 30 MeV.

experimental data for emergent protons at 30° resulting from 325-MeV bremsstrahlung photons on ^{12}C [39] and emergent protons at 60° from 342-MeV bremsstrahlung photons on ^{12}C.[5] The differences in both magnitude add shape of the experimental data are apparent. These differences cannot be attributed entirely to the differences in maximum photon energies. This disagreement in the experimental data is very evident in Fig. 18, in which the calculated energy spectra for two values ($Q = Q_{Schiff}$ and $Q = 2.75$ Q_{Schiff}) are plotted. The degree of agreement between the calculated and experimental values for the higher photon energies considered in these figures appears comparable to the degree of agreement at the lower photon energies.

Cross Sections for Production of Residual Nuclei Resulting from Bremsstrahlung and Monoenergetic Photons on ^{127}I

One of the rewarding aspects of including secondary-particle–nucleus interactions with the quasideuteron

model is that radiochemical cross sections can be obtained. Listed in Table II are the cross sections for the production of various residual nuclei which result from 100-, 200-, and 300-MeV bremsstrahlung photons on ^{127}I.[40] The theoretical bremsstrahlung results have been divided by 1.59 ($Q = 1.59$ Q_{Schiff}). The $\sigma(\gamma, 2n)$ cross section was not measured experimentally[40] and therefore is not listed. Also, the threshold value of the $\sigma(\gamma, n)$ cross section lies in the photon energy region (giant dipole resonance region) in which it is felt that the quasideuteron interaction is not the major mode of initial photon nuclear interaction and, therefore, comparisons were not made for this cross section. The over-all agreement between the calculated and experimental values is good particularly when one realizes that there may be some difference between the experimental photon spectrum and that used in the calculations.

Listed in Table III are data representing monoenergetic photons on ^{127}I. The $\sigma(\gamma, n)$ cross sections are not

[39] B. T. Feld et al., Phys. Rev. **94**, 1000 (1954).

[40] G. G. Jonsson and B. Forkman, Nucl. Phys. **A107**, 52 (1968).
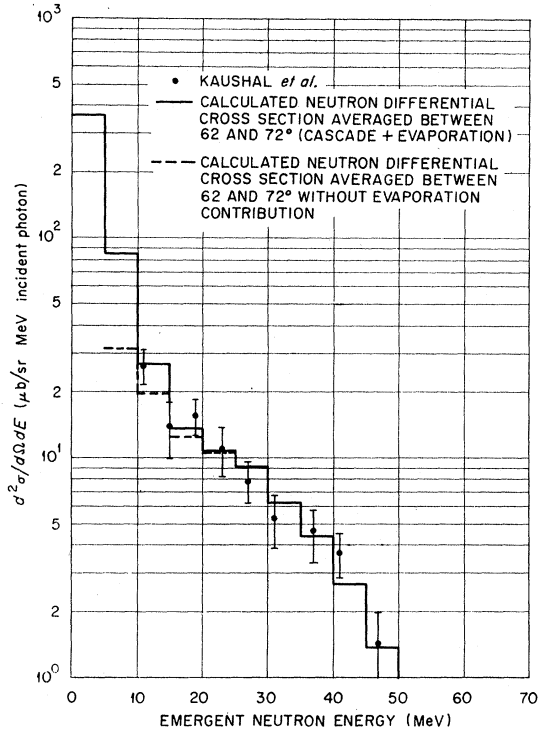
FIG. 8. Differential neutron energy spectrum at 67.5° resulting from (85, 55)-MeV bremsstrahlung-difference photons on ^{63}Cu showing the evaporation contribution.
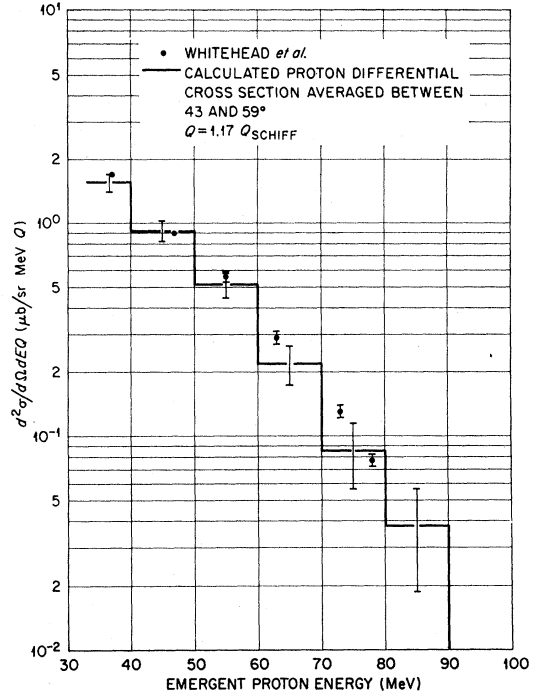
FIG. 10. Differential proton energy spectrum at 51.4° resulting from 110-MeV bremsstrahlung photons on ^{12}C.
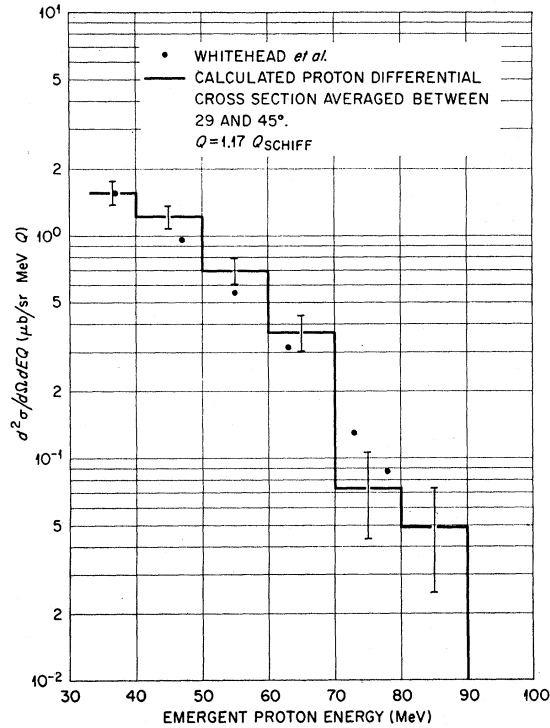
FIG. 9. Differential proton energy spectrum at 36.5° resulting from 110-MeV bremsstrahlung photons on ^{12}C.
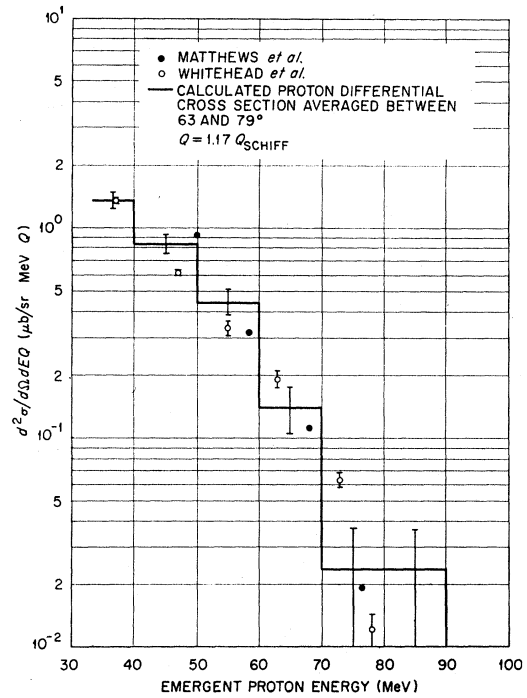
FIG. 11. Differential proton energy spectrum at 71.2° resulting from 110-MeV bremsstrahlung photons on ^{12}C.
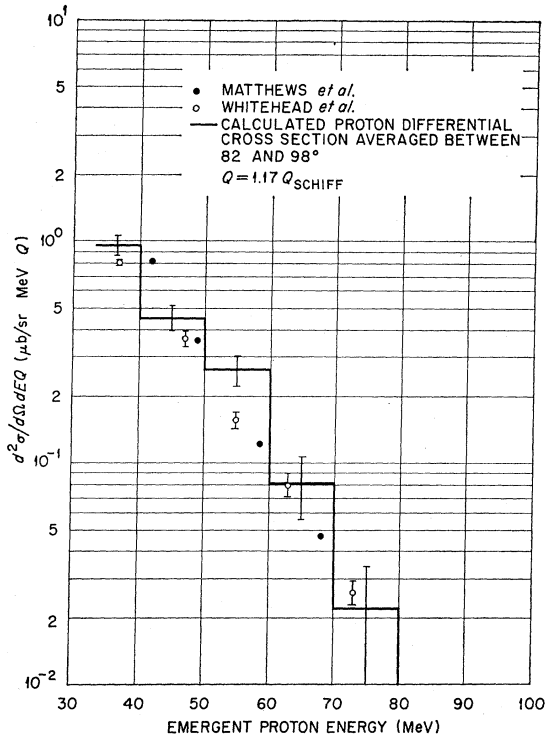
FIG. 12. Differential proton energy spectrum at 90° resulting from 110-MeV bremsstrahlung photons on ^{12}C.
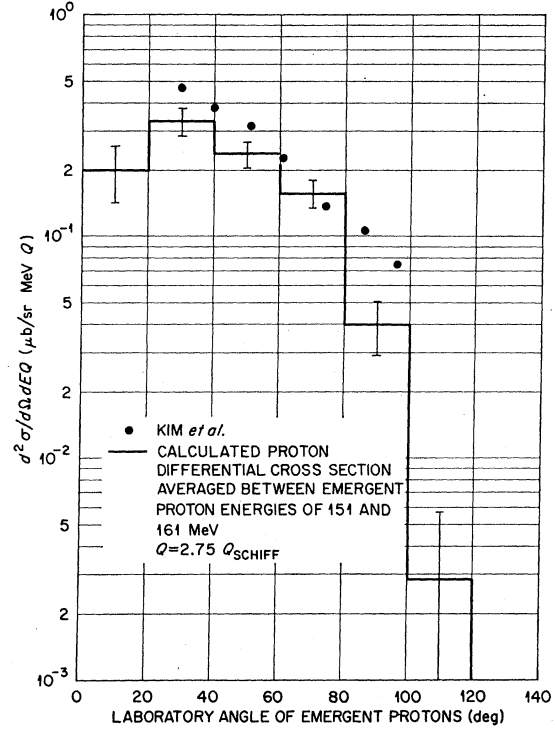
FIG. 14. Differential proton angular distribution for 156-MeV protons resulting from 335-MeV bremsstrahlung on ^{12}C.
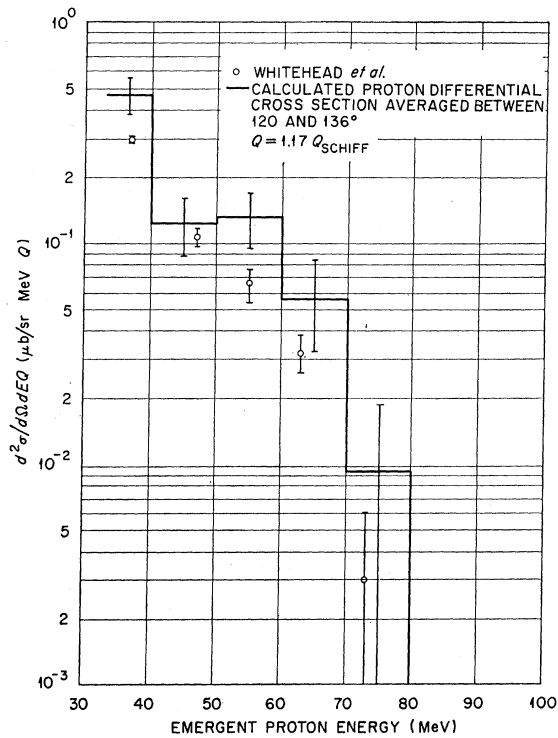
FIG. 13. Differential proton energy spectrum at 128.6° resulting from 110-MeV bremsstrahlung photons on ^{12}C.
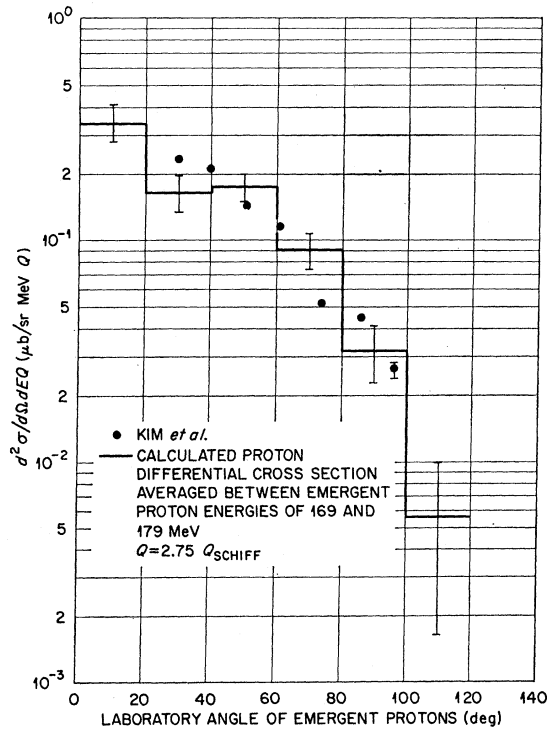
FIG. 15. Differential proton angular distribution for 174-MeV protons resulting from 335-MeV bremsstrahlung on ^{12}C.
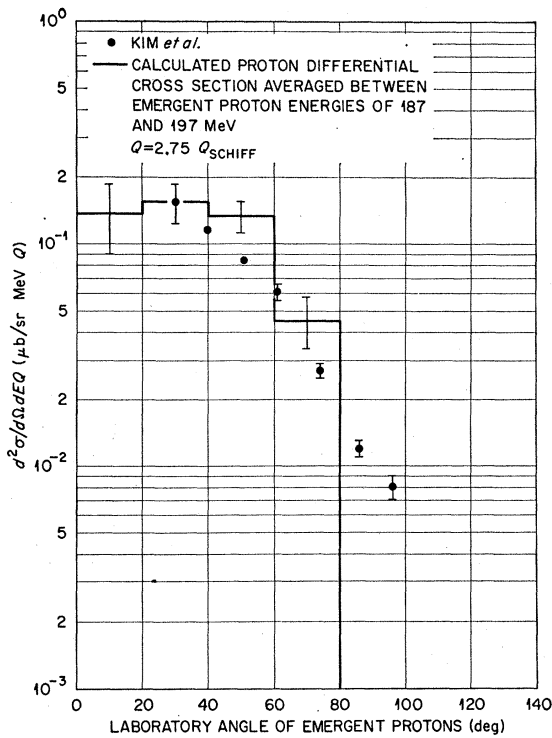
FIG. 16. Differential proton angular distribution for 192-MeV protons resulting from 335-MeV bremsstrahlung on ^{12}C.
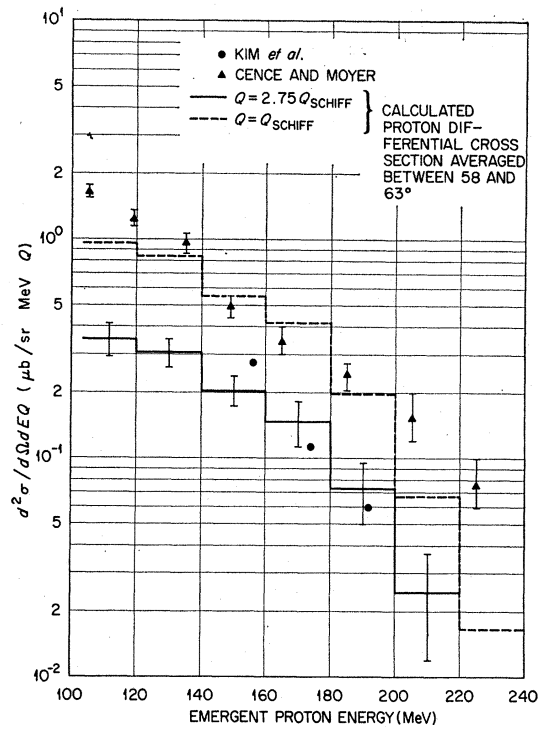
FIG. 18. Differential proton energy spectrum at 60° resulting from 335-MeV bremsstrahlung on ^{12}C.
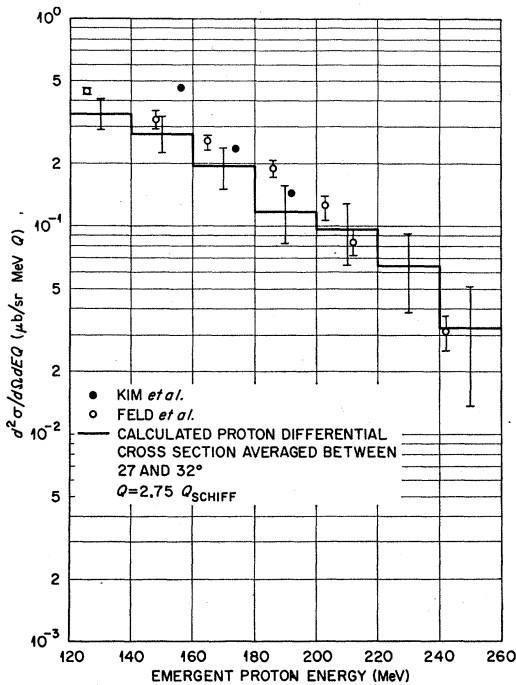
FIG. 17. Differential proton energy spectrum at 30° resulting from 335-MeV bremsstrahlung on ^{12}C.
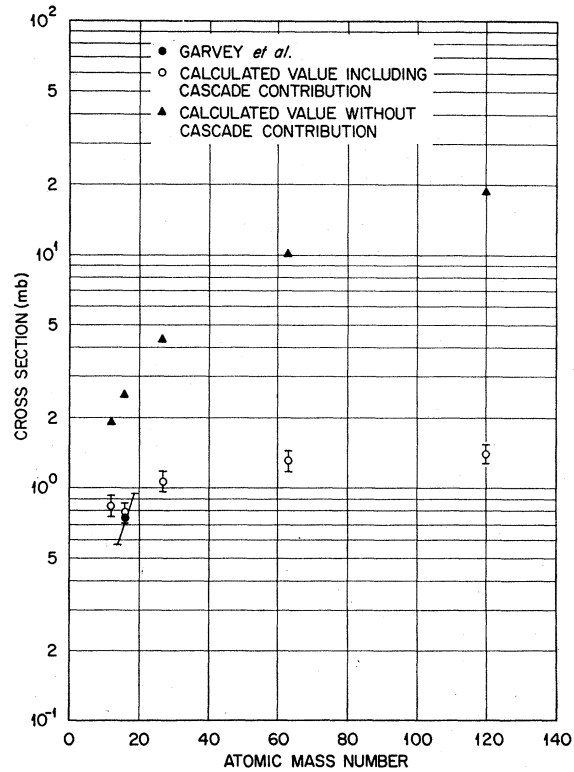
FIG. 19. Total cross sections for observing neutron-proton coincidences which result from 250-MeV photons incident on selected elements.

TABLE II. Total cross sections for the production of various residual nuclei resulting from bremsstrahlung photons on ^{127}I.

Maximum photon energy (MeV)	Type of interaction	Theoret cross sections[a] (mb/Q)	Expt cross sections[b] (mb/Q)
100			
	$\sigma(\gamma, 3n)$	4.22	5.2
	$\sigma(\gamma, 4n)$	2.75	2.3
	$\sigma(\gamma, 5n)$	1.86	1.3[c]
	$\sigma(\gamma, 6n)$	1.18	0.41
	$\sigma(\gamma, 7n)$	0.46	0.19
		10.46	9.4
200			
	$\sigma(\gamma, 3n)$	4.56	6.6
	$\sigma(\gamma, 4n)$	3.48	3.9
	$\sigma(\gamma, 5n)$	2.56	1.9[c]
	$\sigma(\gamma, 6n)$	1.31	0.75
	$\sigma(\gamma, 7n)$	0.74	0.39
		12.65	13.5
300			
	$\sigma(\gamma, 3n)$	5.42	7.2
	$\sigma(\gamma, 4n)$	3.91	4.7
	$\sigma(\gamma, 5n)$	2.89	2.3[c]
	$\sigma(\gamma, 6n)$	1.73	1.2
	$\sigma(\gamma, 7n)$	1.29	0.56
		15.24	16.0

[a] $Q = 1.59Q_{Schiff}$.
[b] G. G. Jonsson and B. Forkman, Nucl. Phys. **A107**, 52 (1968).
[c] These values have been estimated by G. G. Jonsson and B. Forkman (see Ref. b).

listed because of the extremely large values determined by the experimentalist and the correspondingly small values obtained from the theoretical calculations. For example, for photon energies between 200 and 300 MeV, the experimental value is between 10 and 20 mb while the calculated value for this range in photon energy is 0.5 mb. As the experimenters[40] have pointed out, these monoenergetic photon data must be considered to be very approximate. However, it is interesting to note that both the calculated and experimental sums of the different cross sections have the same trend as a function of photon energy.

Cross Sections for Observing Neutron-Proton Coincidences

The standard procedure for determining the quasi-deuteron constant is to observe neutron-proton coincidences. The calculated cross sections for observing such coincidences for selected elements are shown in Fig. 19. The incident photon energy is 250 MeV. The open circles represent the calculated values with the

cascade contribution and the open triangles represent the calculated values without the cascade contribution. The increase in the ^{12}C cross section is probably due to statistical fluxuation. The experimental data are by Garvey et al.[8] Another set of experimental data by

TABLE III. Total cross sections for the production of various residual nuclei resulting from monoenergetic photons on ^{127}I.

Photon energy (MeV)	Type of interaction	Theoret cross sections (mb)	Expt cross sections[a] (mb)
50			
	$\sigma(\gamma, 3n)$	2.07	2.0
	$\sigma(\gamma, 4n)$	12.38	2.4
	$\sigma(\gamma, 6n)$	0	0
	$\sigma(\gamma, 7n)$	0	0
		14.45	4.4
100			
	$\sigma(\gamma, 3n)$	0.33	0.52
	$\sigma(\gamma, 4n)$	0.46	1.0
	$\sigma(\gamma, 6n)$	1.09	0.56
	$\sigma(\gamma, 7n)$	1.49	0.39
		3.37	2.5
150			
	$\sigma(\gamma, 3n)$	0.17	0.53
	$\sigma(\gamma, 4n)$	0.30	1.0
	$\sigma(\gamma, 6n)$	0.51	0.36
	$\sigma(\gamma, 7n)$	0.61	0.20
		1.59	2.1
200			
	$\sigma(\gamma, 3n)$	0.71	0.78
	$\sigma(\gamma, 4n)$	0.41	1.0
	$\sigma(\gamma, 6n)$	0.30	0.45
	$\sigma(\gamma, 7n)$	0.53	0.16
		2.05	2.4
250			
	$\sigma(\gamma, 3n)$	1.19	1.2
	$\sigma(\gamma, 4n)$	1.15	1.0
	$\sigma(\gamma, 6n)$	1.19	0.83
	$\sigma(\gamma, 7n)$	1.45	0.43
		4.98	3.5
300			
	$\sigma(\gamma, 3n)$	1.25	1.6
	$\sigma(\gamma, 4n)$	1.15	1.1
	$\sigma(\gamma, 6n)$	1.04	0.94
	$\sigma(\gamma, 7n)$	1.45	0.64
		4.89	4.3

[a] G. G. Jonsson and B. Forkman, Nucl. Phys. **A107**, 52 (1968).

Stein et al.[41] is available, but these data seem inconsistent with more recent measurements. Garvey et al.[8] give an energy argument that satisfactorily explains the consistently low experimental values of Stein et al.[41] When the experimental data of Garvey et al.[8] were modified to account for secondary-particle–nuclear interactions, the quasideuteron constant that was obtained was 10.3. This is the same value used in the present calculations. As can be seen, however, excellent agreement was obtained between the unmodified experimental data and the calculated data, showing clearly that the Serber model can accurately account for the secondary-particle–nucleus interactions.
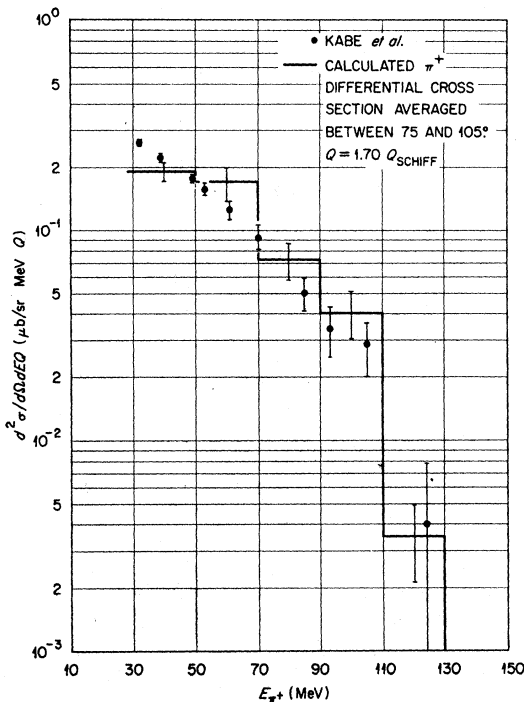
FIG. 20. Differential positive-pion energy spectrum at 90° resulting from 305-MeV bremsstrahlung photons on ^{12}C.

Positive Pions from 305-MeV Bremsstrahlung Photons on ^{12}C

In Fig. 20, the calculated positive-pion energy spectrum at 90° resulting from 305-MeV bremsstrahlung on ^{12}C and the experimental results of Kabe et al.[42] are compared. The calculated values have been divided by 1.70 ($Q = 1.70\ Q_{Schiff}$). The shapes of the two energy spectra are in favorable agreement. Since the experiment gives the energy spectrum at only one angle, no conclusive comment can be made about the angular distribution used in the calculations for pion emission resulting from photon-nucleon interactions.

[41] P. C. Stein et al., Phys. Rev. **119**, 348 (1960).
[42] S. Kabe et al., J. Phys. Soc. Japan **19**, 1800 (1964).
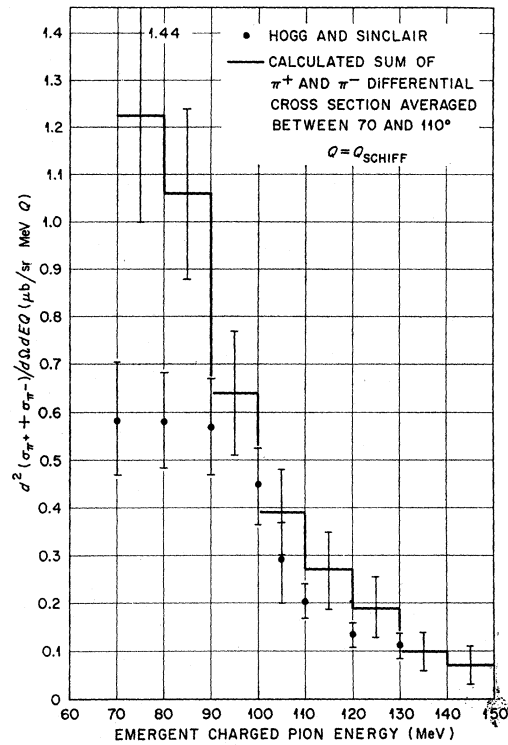
FIG. 21. Differential charged-pion energy spectrum at 90° resulting from 330-MeV bremsstrahlung photons on ^{40}Ca.

Positive and Negative Pions from 330-MeV Bremsstrahlung Photons on ^{40}Ca

Shown in Fig. 21 is a comparison between the calculated sum of the differential negative- and positive-pion energy spectra at 90° resulting from 330-MeV bremsstrahlung photons on ^{40}Ca and the experimental results of Hogg and Sinclair.[43] It is to be noted that in this case no renormalization of the calculations was
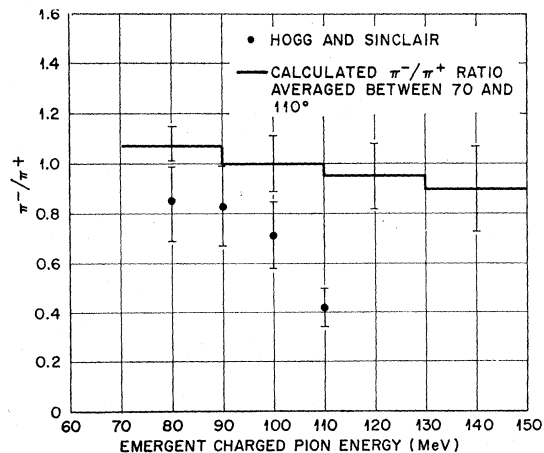
FIG. 22. Ratio of π^- to π^+ yield at 90° resulting from 330-MeV bremsstrahlung photons on ^{40}Ca.

[43] W. R. Hogg and D. Sinclair, Phil. Mag. **1**, 466 (1956).
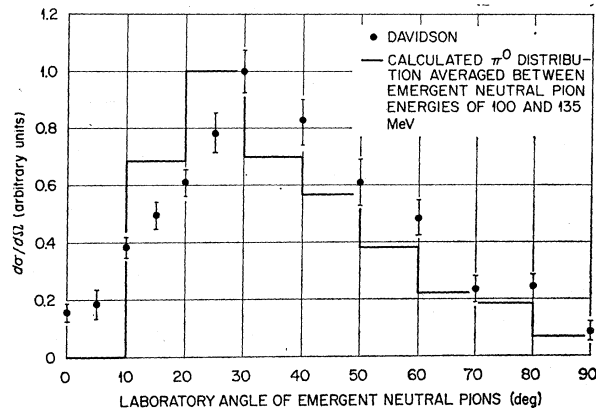
FIG. 23. Differential neutral-pion angular distribution for 115-MeV neutral pions resulting from 280-MeV bremsstrahlung on ^{12}C.

necessary. Shown in Fig. 22 is a comparison of the π^- to π^+ differential cross-section ratio and the data of Hogg and Sinclair.[43] The agreement is reasonable for both the charged-pion energy spectrum and the π^- to π^+ differential cross-section ratio.

Neutral Pions from 280-MeV Bremsstrahlung Photons on ^{12}C, ^{27}Al, and ^{63}Cu

Comparisons of the calculated angular distributions for 115-MeV neutral pions from 180-MeV bremsstrahlung photons on ^{12}C, ^{27}Al, and ^{63}Cu and the experimental results of Davidson[44] are shown in Figs. 23–25. The agreement is good for ^{12}C and ^{27}Al and fair for ^{63}Cu. The loss of pions in the forward direction is due to the
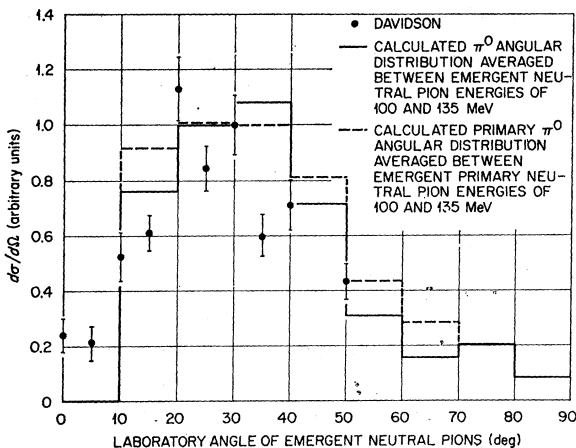
FIG. 24. Differential neutral pion angular distribution for 115-MeV neutral pions resulting from 280-MeV bremsstrahlung on ^{27}Al.

exclusion principle.[24,45] The dashed line in Fig. 24 represents the angular distribution of the primary-cascade neutral pions. Only the shapes of the two calculated spectra can be compared since they are both plotted with arbitrary scales. The basic shape of the calculated primary π^0 angular distribution is not significantly altered by secondary interactions at this pion energy.

CONCLUSIONS

It has been shown by the over-all agreement between the calculations and the various types of experimental data that the quasideuteron model and single-pion production when coupled with the intranuclear-cascade model can be used to predict reliable information concerning photon-nucleus interactions over a very wide range in atomic mass numbers ($\gtrsim 12$) and over a wide
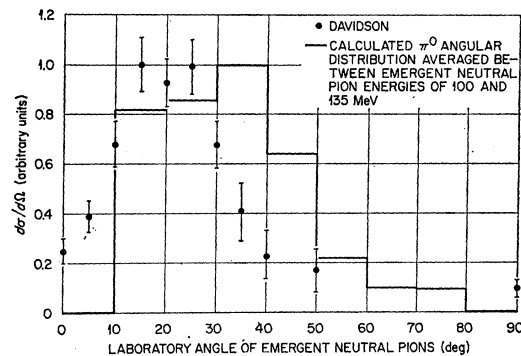
FIG. 25. Differential neutral-pion angular distribution for 115-MeV neutral pions resulting 280-MeV bremsstrahlung photons on ^{63}Cu.

range in photon energy (~ 40–~ 350 MeV). The calculations indicate that the quasideuteron constant L is, to a very good approximation, independent of photon energy and atomic mass number, and that the quasideuteron interaction, which was originally developed for photon energies above 150 MeV, is still the major interaction mode for photon energies as low as 40 MeV. Exactly how low in photon energy this interaction mechanism can be used remains to be determined.

ACKNOWLEDGMENTS

[44] G. Davidson, dissertation, Massachusetts Institute of Technology, 1957 (unpublished).

[45] C. D. Zerby et al., Oak Ridge National Laboratory Report No. ORNL-CF-61-7-20, 1961 (unpublished).